Chemical and Process Engineering 2014, 35 (1), 137-147
DOI: 10.2478/cpe-2014-0010

# STUDY OF THE TURBULENT FLOW STRUCTURE AROUND A STANDARD RUSHTON IMPELLER

Bohuš Kysela*[1], Jiří Konfršt[1], Ivan Fořt[2], Michal Kotek[3], Zdeněk Chára[1]

[1]Institute of Hydrodynamics AS CR, v. v. i., Pod Patankou 30/5, Prague, Czech Republic

[2]Czech Technical University in Prague, Faculty of Mechanical Engineering, Department of Process Engineering, Technicka 4, Prague, Czech Republic

[3]Technical University of Liberec, Institute for Nanomaterials, Advanced Technology and Innovation, Studentska 1402/2, Liberec, Czech Republic

The velocity field around the standard Rushton turbine was investigated by the Laser Doppler Anemometry (LDA) and Particle Image Velocimetry (PIV) measurements. The mean ensemble-averaged velocity profiles and root mean square values of fluctuations were evaluated at two different regions. The first one was in the discharge stream in the radial direction from the impeller where the radial flow is dominant and it is commonly modelled as a swirling turbulent jet. The validity range of the turbulent jet model was studied. The second evaluated region is under the impeller where flow seems to be at first sight rather rigorous but obtained results show nonnegligible values of fluctuation velocity.

**Keywords:** Rushton turbine, mixing, ensemble-average mean velocity, fluctuation velocity LDA/LDV, PIV, velocity profiles

## 1. INTRODUCTION

The knowledge of flow and its turbulent behaviour inside an agitated vessel is crucial for a better understanding of mixing processes, scale-up modelling, geometry improvement, etc. The flow in a cylindrical agitated vessel should be divided into several regions where the flow behaviour is quite different. The vicinity of impeller blades is of particular significance where shear and dissipation rates reach high values. The velocity profile in the stream induced by a standard Rushton turbine can be modelled as a tangential cylindrical jet (Cutter, 1966). The proposed model was compared with experimental results of the mean ensemble-averaged velocity (Drbohlav et al, 1978; Fořt et al, 1979; Obeid et al., 1983; Talaga and Fořt, 2012). The mean ensemble-averaged velocity and fluctuation velocity profiles in the impeller outflow stream were investigated also by many other authors e.g. (Bittins and Zehner, 1977; Devi and Kumar, 2013; Kratěna and Fořt, 2004; Schafer et. al., 1997; Venneker et al., 2010; Wu and Paterson, 1998), while the region under impeller has not been treated with the same interest. However, it might be useful for a comparison of flow regimes, dissipation modelling etc., because the flow under the impeller seems to be stable and isotropic. Hence we measured and analysed velocity profiles and namely their fluctuation values in both regions.

*Corresponding author, e-mail: kysela@ih.cas.cz

## 2. A MODEL OF VELOCITY PROFILES IN THE DISCHARGE STREAM

Based on the presumption that the standard Rushton impeller is replaced with a tangential cylindrical jet, see Fig 1 (Cutter, 1966), the radial component of the discharge flow was derived in a dimensionless form, $W_r^* = f(z^*)$, for various dimensionless coordinates $r^* = 2r/D$, where the dimensionless $z^*$ axial coordinate is the distance from the impeller disk axis normalised by the half-height of the blade. The radial component of the mean velocity could be simply expressed in a dimensionless form (Drbohlav et al, 1978):

$$W_r^* = A_1(1 - \tanh[A_2(z^* - A_3)]) \tag{1}$$

where $A_1$, $A_2$ and $A_3$ are parameters for determining the shape of profiles:

$$A_1 = \frac{A}{2\pi Dn}\left(\frac{\sigma}{r^3}\right)^{1/2}(r^2 - a^2)^{1/4} \tag{2}$$

$$A_2 = \frac{\sigma h}{4r} \tag{3}$$

Here the parameter $a$, is the radius of the cylindrical tangential jet (see Fig. 1) determined from the ratio of the radial and tangential velocity components, respectively. For the known tangential component of the mean ensemble-averaged velocity, the parameter $a$ could be derived from the expression (Obeid et al., 1983):

$$\frac{2a}{D} = 2.087 \cdot Re_M^{-0.106} \tag{4}$$

where $Re_M$ is the impeller Reynolds number

$$Re_M = \frac{nD^2\rho}{\mu} \tag{5}$$

and the flow of agitated liquid is considered as fully turbulent ($Re_M > 1.0 \cdot 10^4$).

Both parameters $a$ and $\sigma$ determine the geometry of the modelled tangential jet and accordingly the parameter $A_3$ refers to the displacement of the velocity profile from the horizontal plane $z^* = 0$, which is proportional to the impeller off-bottom clearance. The parameter $A_1$ represents the maximum radial velocity and $A_2$ represents the reciprocal width of the stream normalised by the half-height of the blade (see Fig. 1).

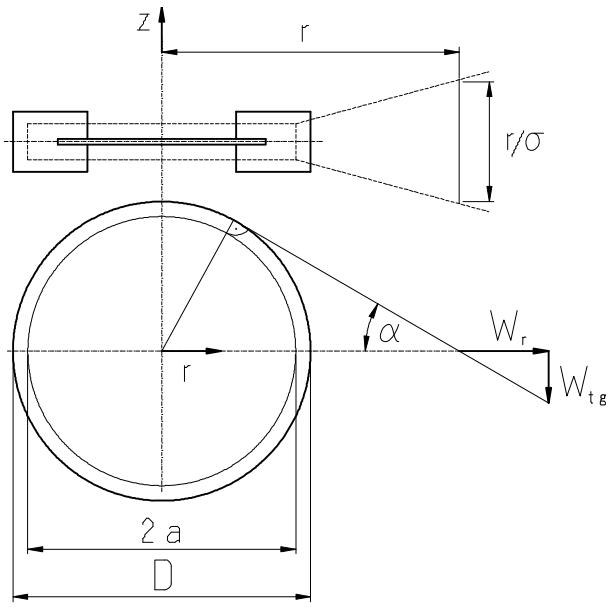


Fig. 1. Geometry of the cylindrical tangential jet

## 3. EXPERIMENTAL

Measurements of velocity profiles were carried out in a flat-bottomed mixing vessel, with water as the working liquid (density $\rho$ = 1000 kg m$^{-3}$, dynamic viscosity $\mu$ = 1 mPa s). The vessel was equipped with four radial baffles and agitated with a six-blade standard Rushton turbine (see Fig. 1). The stirred vessel diameter was $T$ = 300 mm, filled with liquid to the level $H = T$. The diameter of the impeller was $D$ = 100 mm (T/D = 3) and installed with off-bottom clearance $C/D$ = 0.75. The width of baffles was $b$ = 0.1 $T$.

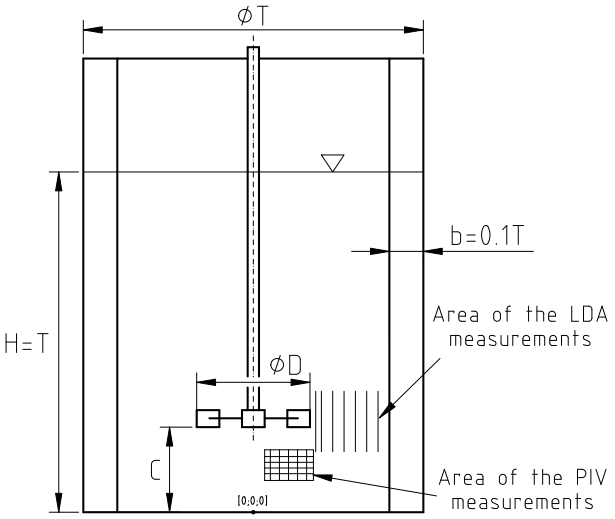


Fig. 2. The pilot plant cylindrical vessel with a six-blade standard Rushton turbine ($T$ = 300 mm, $H/T$ = 1, $C/D$ = 0.75, $b/T$ = 1/10, four baffles)

### *3.1. Laser Doppler Anemometry measurements*

LDA 1D radial velocity measurements in the impeller discharge stream were performed along axial profiles with several distances from the impeller blade (Fig. 2). The values of the dimensionless component $r^* = 2r/D$ were selected as follows: 1.1; 1.2; 1.4; 1.8; 2.0; 2.2. One component LDA system set-up consists of: Coherent INNOVA 305 Ion-Argon laser supply with power 5 W and separated beam only for one component measurement on the wavelength 514.5 nm, DANTEC fiberflow transmitting optics and P80 DANTEC BSA processor. The set-up was supervised by BSA FLOW SOFTWARE v3.0 installed on standard PC where data were processed. S-HGS (Silver coated – Hollow Glass Spheres) with the mean diameter 10 μm and density 1.1 g cm$^{-3}$ were used as trace particles. LDA measurements were carried out for impeller speeds 350 and 400 rpm, when impeller Reynolds number (Eq. 5) equalled to $5.8\times10^4$ and $6.7\times10^4$, respectively.

### *3.2. Particle Image Velocimetry measurements*

Results from the region under the impeller were obtained by the PIV measurement technique. The investigated area was 43x27 mm (Fig. 2). The area was adjusted 10 mm from the shaft axis and 20 mm under the impeller. The PIV system was time-resolved LITRON LDY 304, Nd:YLF laser; high speed camera SpeedSence 611 (with full resolution 1280x800) from DANTEC. Rhodamine B fluorescent particles with the mean diameter 10 μm were used as seeding particles along with a wavelength filter to reduce laser reflections. The system was supervised by the Dynamic software which was also used for velocity evaluation. The final evaluated vector grid was 79×49. The operating frequency was 1 kHz (i.e. 1000 vector fields per second) the record length was 15 s for the impeller speed 600 rpm, when

impeller Reynolds number (Eq. 5) was $1.0\times10^5$. This very impeller speed was chosen because a low level of measurement accuracy below it and because it was impossible for the driver to set up higher impeller speed in our system configuration.

## 4. RESULTS AND DISCUSSION

All obtained experimental data were evaluated as the mean ensemble-averaged velocity profiles and as profiles of root-mean-square (RMS) velocity fluctuations. Results are presented in a dimensionless form where dimensional data are normalised by the impeller tip speed $V_{tip}=\pi Dn$, because the experimental conditions were maintained under the turbulent regime ($Re_M > 10^4$) where velocity is dependent only on the impeller speed.

### *4.1. Profiles of radial velocity component in impeller discharge stream (results of LDA measurements)*

The experimental results of the radial ensemble-averaged mean velocities were fitted with the proposed model Eq. (1). Parameters $A_1$, $A_2$, $A_3$ from a regression are shown in Table 1 and Table 2 for the impeller speeds of 350 rpm and 400 rpm, respectively. The fitted curves to the experimental data are depicted for each dimensionless radius in Figs. 3-8.

The other dimensionless parameters of the model given in Tables 1 and 2 were calculated using Eq. 3 and Eq. 4 with Eq. 2, respectively. For the investigated system the values of parameter $a$, were calculated only from Eq. 4, because in our experiments the tangential (peripheral) component of liquid velocity in the impeller discharge stream was not measured. The parameter $\sigma$ was subsequently derived from Eq. 3 (see Fig 1) using obtained values of the $A_2$ from regressions and parameter $A/2\pi Dn$ was derived using Eq. 2 from obtained values $a$, $\sigma$, $A_1$ respectively. The results calculated for each dimensional radius and both impeller speeds are presented in Table 1 and Table 2.

Table 1. Fitting parameters of Eqs.1-3 derived from the measured mean ensemble-averaged radial velocity data at impeller speed $n$ = 350 rpm; $a$ = 0.0321 (Eq. 4)

| $r^*$ | $A_1$ | $A_2$ | $A_3$ | $\sigma$ | $A/2\pi D^2n$ |
|---|---|---|---|---|---|
| 1.1 | 0.914 | 2.435 | 0.243 | 26.79 | 0.106 |
| 1.2 | 0.895 | 2.017 | 0.366 | 24.20 | 0.122 |
| 1.4 | 0.737 | 1.761 | 0.441 | 22.85 | 0.117 |
| 1.8 | 0.556 | 0.854 | 0.616 | 15.37 | 0.132 |
| 2.0 | 0.504 | 0.681 | 0.681 | 13.62 | 0.140 |
| 2.2 | 0.449 | 0.597 | 0.701 | 13.13 | 0.139 |

Table 2. Fitting parameters of Eqs.1-3 derived from the measured mean ensemble-averaged radial velocity data at impeller speed $n$ = 400 rpm; $a$ = 0.0326 (Eq. 4)

| $r^*$ | $A_1$ | $A_2$ | $A_3$ | $\sigma$ | $A/2\pi D^2n$ |
|---|---|---|---|---|---|
| 1.1 | 0.905 | 2.409 | 0.267 | 26.50 | 0.107 |
| 1.2 | 0.869 | 2.193 | 0.304 | 26.32 | 0.111 |
| 1.4 | 0.747 | 1.583 | 0.398 | 22.16 | 0.118 |
| 1.8 | 0.558 | 0.868 | 0.564 | 15.62 | 0.131 |
| 2.0 | 0.497 | 0.712 | 0.624 | 14.24 | 0.135 |
| 2.2 | 0.438 | 0.602 | 0.682 | 13.24 | 0.135 |

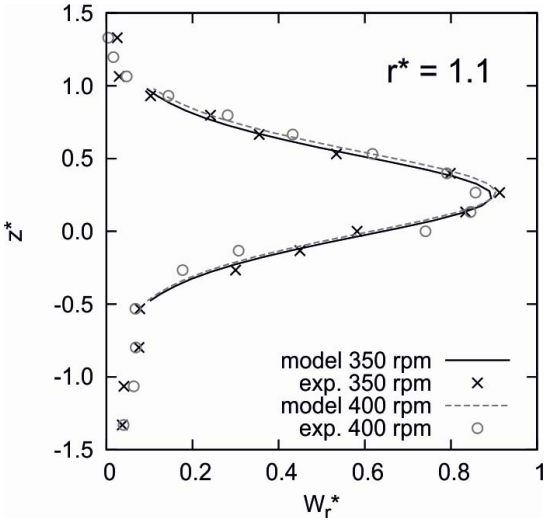


Fig. 3. Radial component of the ensemble-averaged mean velocity at r*=1.1

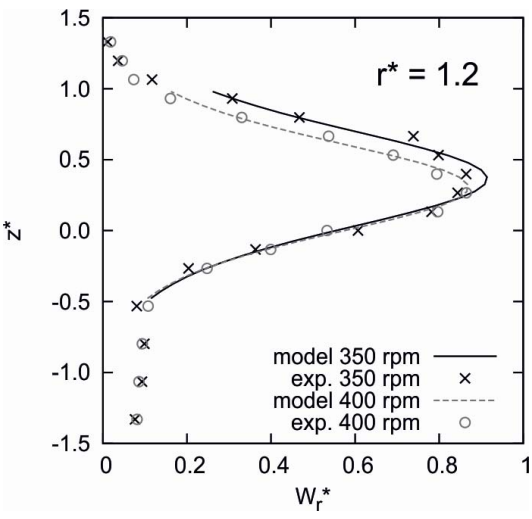


Fig. 4. Radial component of the ensemble-averaged mean velocity at r*=1.2

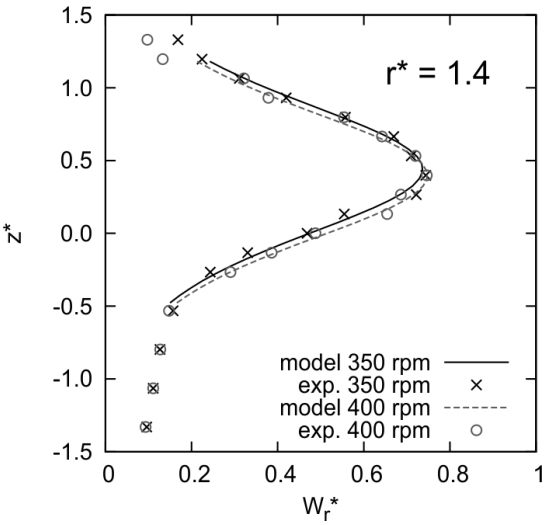


Fig. 5. Radial component of the ensemble-averaged mean velocity at r*=1.4

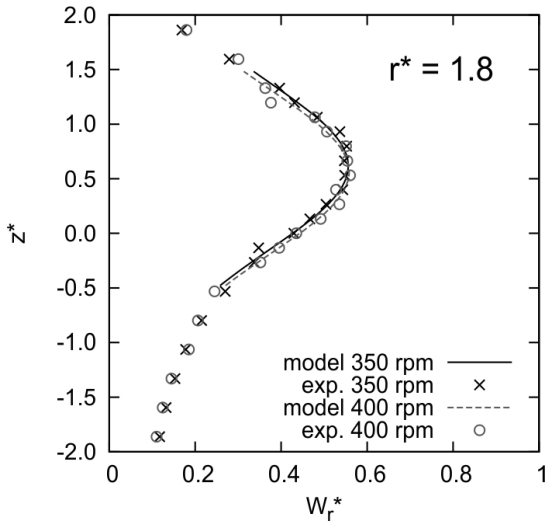


Fig. 6. Radial component of the ensemble-averaged mean velocity at r*=1.8

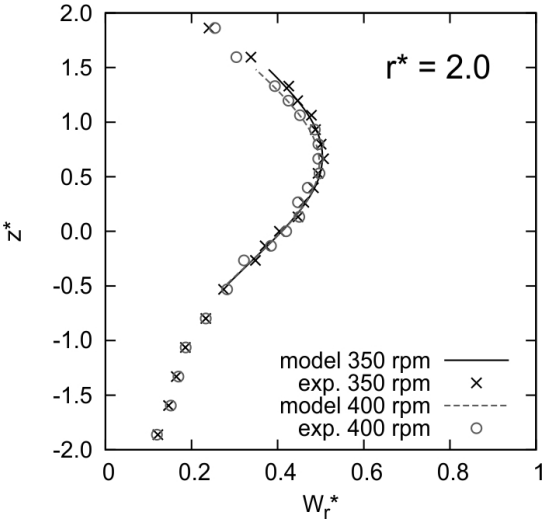


Fig. 7. Radial component of the ensemble-averaged mean velocity at r*=2.0

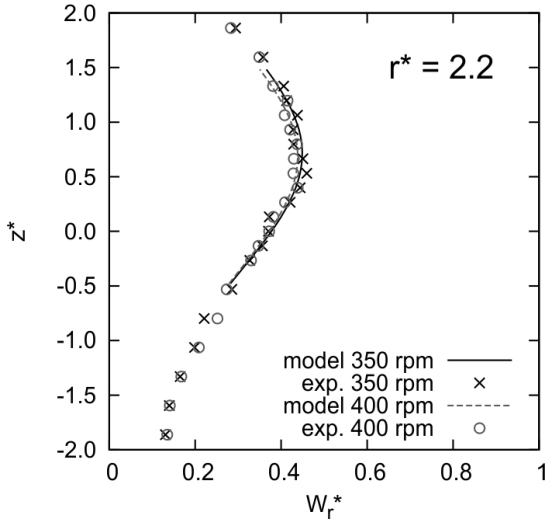


Fig. 8. Radial component of the ensemble-averaged mean velocity at r*=2.2

The radial profiles obtained from LDA measurements confirm that the shape of the profile at each radius corresponds to the bell shape typical for a turbulent jet and is not dependent on the impeller speed. The measured data agree with the proposed model quite well, Figs. 3-8. The fitted data of the cylindrical tangential jet model are summarised in Tables 1 and 2. On the basis of the fitted data the profiles could be divided into two zones - the zone of the flow establishment (ZFE) for $r^*$: 1.1; 1.2; 1.4 and the zone of established flow (ZEF) for $r^*$: 1.8; 2.0; 2.2 (Ben-Nun and Sheintuch, 2013). The parameters $\sigma$ and $A/2\pi D^2 n$, characterising a standard Rushton impeller as a tangential axially symmetrical jet, show week dependence of coordinate $r^*$ in ZFE (see Tables 1 and 2), but on the contrary, they depend on $r^*$ in ZEF. A similar behaviour of the two different flow regimes is also shown on the profiles of the r. m. s. values for the fluctuation velocities in Fig 9. While the fluctuations profiles in ZFE attained the same maximum values and have a similar shape, the fluctuation values in ZEF decrease and the profiles are dispersed. A comparison of both impeller speeds of the fluctuation values in ZFE is depicted in Fig 10, where the fluctuation velocity independency on the Reynolds number is also obvious. The explanation of differences between the axial profiles of the r.m.s. values in ZFE and ZEF zones follows from two major phenomena: the jet development of profiles from ZFE to the self-similar ones of the second zone ZEF and existence of the pseudo-turbulence in former zone. The periodic component of the turbulence spectra corresponding to the frequency of impeller blades (Wu and Paterson, 1998) significantly deviates the spectrum of kinetic energy of the turbulence from its course under random fluctuations only. It is useful to point out that, similarly as for axial profiles of the ensemble-averaged velocity in the impeller discharge stream, the r.m.s. velocity profiles exhibit the axial deviation above the plane of the impeller disc (see Figs. 9 and 10). This phenomenon coincides with a non-symmetrical position of the (off-bottom clearance) of the impeller in an agitated system.

The results of the characteristic coefficients of the modelled tangential turbulent jet were summarised by several authors in (Talaga and Fořt, 2012). The values of the dimensionless complex $A/2\pi D^2 n$ are in good agreement with other measurements for similar geometry where $D/T = 1/3$, while the values of the $\sigma$ are approximately about 30 % higher (in the ZEF) than those summarised in (Talaga and Fořt, 2012). It should probably be caused by dissimilarity of the mixing vessel geometries, namely different impeller off-bottom clearance.

The axial displacement of the velocity profile maximum is proportional to the parameter $A_3 \approx z^*\left(W^*_{r,MAX}\right)$ in Eq. 1. The values of this parameter are dependent on the dimensionless radius $r^*$ and the subsequent numerical values of the power expression in power form are depicted in Fig. 11. The resulting regression curve can be approximated as:

$$A_3 = 0.26\ (r^*)^{1.30} \tag{6}$$

This resulting curve is not consistent with a dependency obtained by Talaga and Fořt (2012) where the power exponent amounts to almost five, whereas our results show a real tendency, where the axial displacement of the profile maximum depends on the impeller off-bottom clearance. The lower the impeller off-bottom clearance the higher the axial displacement of the profile maximum above the horizontal plane of the impeller disc (coordinate $z^*$) see e.g. Fig. 3. Therefore, for the used lower value of the impeller off-bottom clearance the radial velocity profiles in stream induced from the standard Rushton turbine are deformed earlier and more gradually. The dependency of the parameter $A_2$ on a dimensionless radius $r^*$ is depicted in Fig. 12. The data points for both investigated impeller speeds are well fitted by the power curve with the exponent equal to -2. The dependency of the parameter $A_1$ on the dimensionless radius $r^*$ development as the results presented shows similar by Ben-Nun and Sheintuch, (2013) where the fitted curve is proportional to the reciprocal value of the dimensionless radius $r^*$. These results indicate that generally higher values of the dimensionless radial velocity were measured for the applied geometry in this experimental investigation.

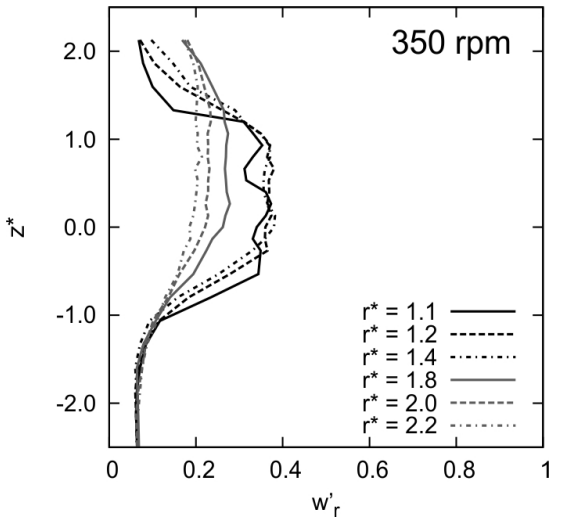


Fig. 9. Axial profiles of the r. m. s. values of the radial fluctuating velocity for the impeller speed 350 rpm

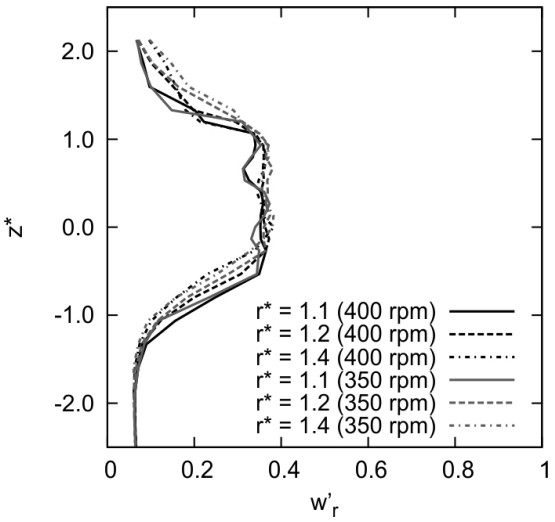


Fig. 10. Comparison of the axial profiles of the r. m. s. values for both impeller investigated speeds in ZFE

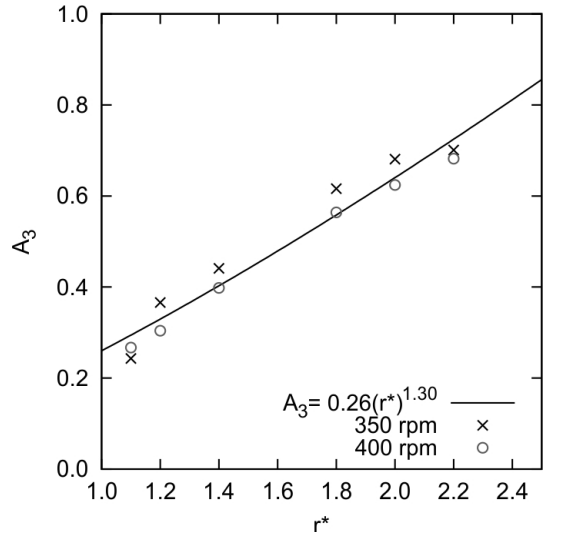


Fig. 11. Axial position of the mean radial velocity maximum $A_3$ of the fitted velocity profiles for both investigated impeller speeds

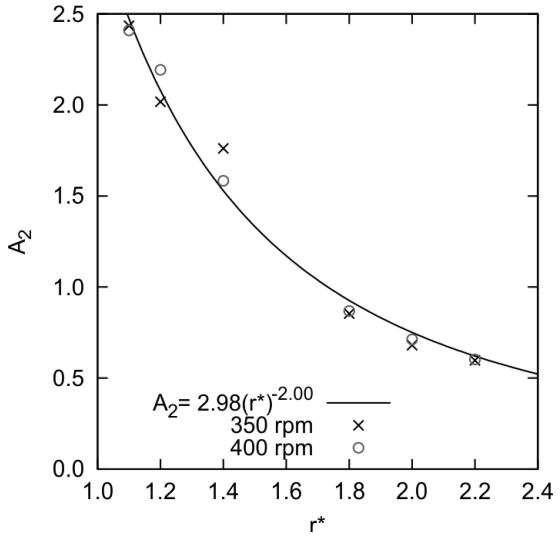


Fig. 12. Relation of the coefficient $A_2$ on the dimensionless radius $r^*$ for both investigated impeller speeds

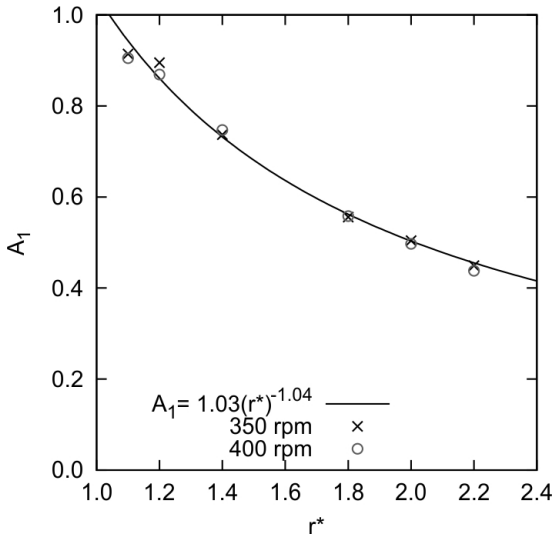


Fig. 13. Relation of the coefficient $A_1$ on the dimensionless radius $r^*$ for both investigated impeller speeds

### *4.2. Velocities under the Rushton turbine (results of PIV measurements)*

The flow under the radial impeller represented by a standard Rushton turbine is considered as an undisturbed homogeneous flow contrary to the impeller discharge stream where three dimensional trailing vortices affect the flow e.g. (Derksen et al., 1999; Ranade et al., 2001). Hence, the region under the impeller seems to be useful for comparisons of turbulence flow changes dependent on operating conditions. The flow was analysed by the time-resolved PIV measurements in this region. The vector field with the mean values of radial and axial components of velocity is depicted in Fig. 14. The size of the vectors is related to the impeller tip speed depicted as the vector on the right side. The axial coordinate $z$ is normalised by the mixing vessel height $H$ and the radial coordinate is the dimensionless radius $r^*$. Four selected profiles of the axial mean ensemble-averaged velocities are shown in Fig. 15. The value of the axial velocity slightly increases with a shorter distance to the impeller and with a longer distance from the impeller axis. The r. m. s. values of the fluctuating velocity are higher in the vicinity of the impeller axis which is probably caused by the flow generated by the impeller shaft tip, while lower values represent the velocity field in the up-flow of the circulation loop. The circulation loop shape is also obvious from the results of the radial component of the mean ensemble-averaged velocities in Fig. 17, where the values in lower positions are lower (the positive direction of the velocity is from the impeller axis to the vessel wall); which means that the radial flow changes ultimately its orientation to the axial direction.

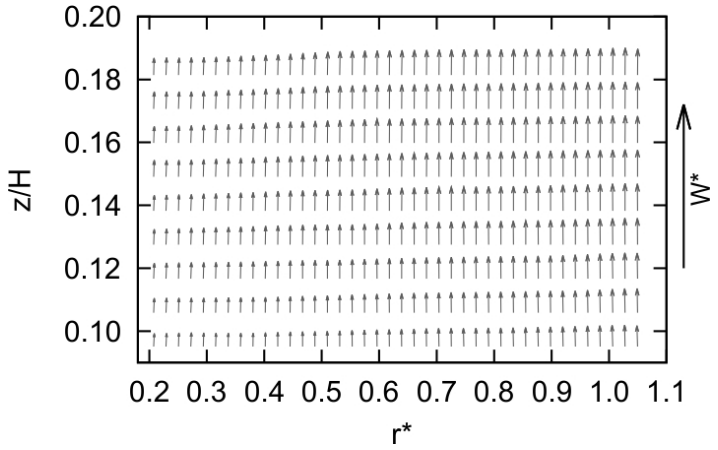


Fig. 14. Vector field of the mean ensemble-averaged velocity under the Rushton turbine impeller.

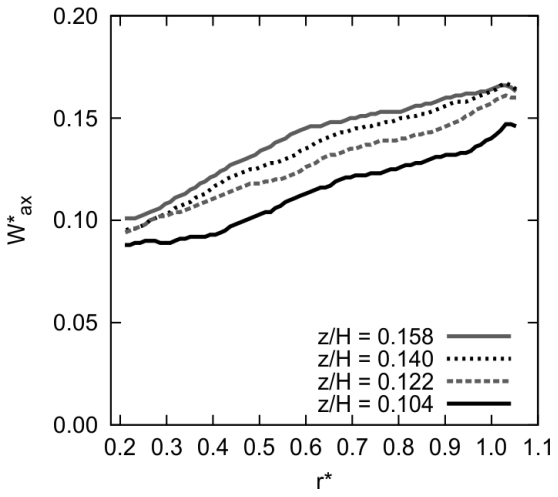


Fig. 15. Axial component of the mean ensemble-averaged velocity under the impeller

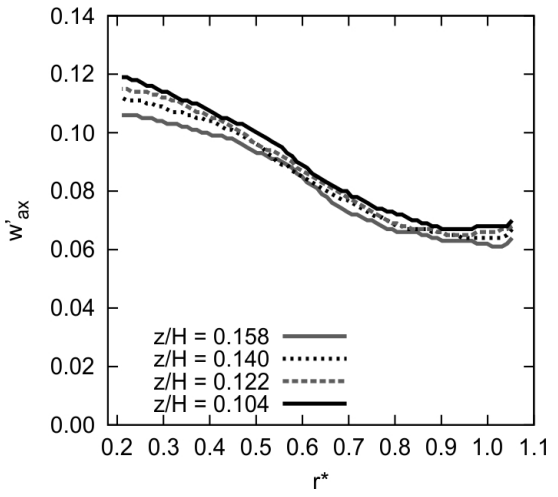


Fig. 16. Axial component of the r. m. s. values of the velocity under the impeller

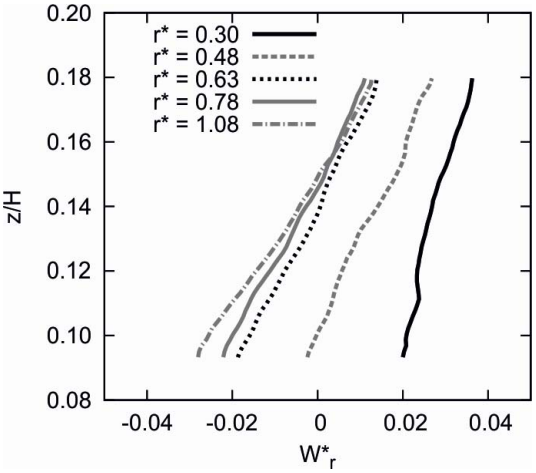


Fig. 17. Radial component of the mean ensemble averaged velocity under the impeller

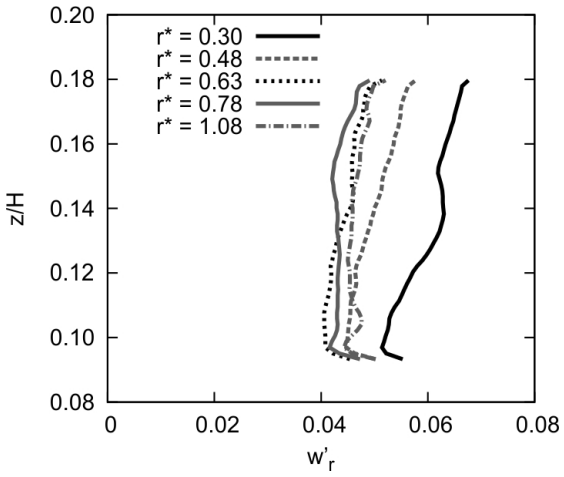


Fig. 18. Radial component of the r. m. s. values of the velocity under the impeller

The analysis of the flow under the impeller demonstrates that the flow attains rather lower values of the mean velocity and lower fluctuation values although the ratio between fluctuations and mean values seems to be rather high.

## 5. CONCLUSIONS

The measured radial velocity profiles are independent of the Reynolds number in the discharged stream from a standard Rushton impeller. LDA measurement data were compared with a model of the cylindrical turbulent tangential jet and the model was found to be in a good agreement with the obtained data. The model fitting and other data analysis supported the theories of the zone of the flow establishment (ZFE) and the zone of the established flow (ZEF). The experimental results reveal a transient region between the zones at the dimensionless radius $r^*$ from 1.4 to 1.8.

The values of the mean radial ensemble-averaged velocity in the impeller discharge stream attain more than 90 % of the impeller tip speed and r.m.s. velocity fluctuations amounting to about 40 %, while in the region under the impeller the values of the mean axial ensemble-averaged velocity reach from 10 % to 17 % (fluctuations 6-12 %) and the value of the radial component is up to 4 % (fluctuations 4-7 %).

The flow in the region under the impeller seems to be rather homogeneous with low velocity values in comparison with the flow in the impeller discharge steam. However, it is necessary to perform long-term measurements, because fluctuations are relatively slow in the region.

*This research has been subsidised by the research project No. GA CR P101/12/2274 and RVO: 67985874.*

## SYMBOLS

| | |
|---|---|
| $A$ | parameter of radial velocity component profile, $m^2\ s^{-1}$ |
| $A_1$ | dimensionless parameter of radial velocity component profile |
| $A_2$ | dimensionless parameter of radial velocity component profile |
| $A_3$ | dimensionless parameter of radial velocity component profile |
| $a$ | radius of cylindrical tangential jet, m |

| | |
|---|---|
| $b$ | width of radial baffle, m |
| $C$ | impeller off-bottom clearance, m |
| $D$ | impeller diameter, m |
| $H$ | height of agitated charge above vessel bottom, m |
| $h$ | impeller blade width, m |
| $n$ | impeller speed, $s^{-1}$ |
| $r$ | dimensional longitudinal (radial) coordinate, m |
| $r^*$ | dimensionless longitudinal (radial) coordinate |
| $T$ | mixing vessel diameter, m |
| $V_{tip}$ | impeller tip velocity, m $s^{-1}$ |
| $W$ | ensemble-averaged mean velocity, m $s^{-1}$ |
| $W^*$ | dimensionless ensemble-averaged mean velocity |
| $w'$ | dimensionless root mean square value of the fluctuating velocity |
| $z$ | dimensional longitudinal (axial) coordinate, m |
| $z^*$ | dimensionless longitudinal (axial) coordinate |

*Greek symbols*

| | |
|---|---|
| $\mu$ | dynamic viscosity, Pa s |
| $\rho$ | density, kg $m^{-3}$ |
| $\sigma$ | dimensionless parameter of mean radial velocity profile |

*Subscripts*

| | |
|---|---|
| $r$ | radial component |
| $ax$ | axial component |
| $tg$ | tangential component |

## REFERENCES


Ben-Nun R., Sheintuch M., 2013. Characterizing turbulent jet properties of radial discharge impeller: potential core, spreading rate and averaged flow field parameters. *9th European Congress of Chemical Engineering*, The Hague (NL), April 2013.

Bittins K., Zehner P., 1994. Power and discharge numbers of radial-flow impellers, Fluid-dynamic interactions between impeller and baffles. *Chem. Eng. Proc.*, 33, 295-301. DOI: 10.1016/0255-2701(94)01011-0.

Cutter L.A., 1966. Flow and turbulence in stirred vessels. *AICHE J.*, 12, 35-44.

Derksen J.J., Doelman M.S., Van den Akker H.E.A., 1999. Three-dimensional LDA measurement in the impeller region of a turbulently stirred tank. *Exp. Fluids*, 27, 522 -532. DOI: 10.1007/S003480050376.

Devi T.T., Kumar B., 2013. Comparison of flow patterns of dual Rushton and CD-6 impellers. *Theor. Fund. Chem. Eng.*, 47, 344-355. DOI: 10.1134/S0040579513040210.

Drbohlav J., Fořt I., Krátký J., 1978. Turbine impeller as a tangential cylindrical jet. *Coll. Czech. Chem. Commun.*, 43, 696-719.

Drbohlav J., Fořt I., Máca K., Ptáček J., 1978. Turbulent characteristics of discharge flow from turbine impeller. *Coll. Czech. Chem. Commun.*, 43, 3148-3161.

Fořt I., Möckel H. O., Drbohlav J., Hrach M., 1979. The flow of liquid in a stream from the standard turbine impeller. *Coll. Czech. Chem. Commun.*, 44, 700-710.

Kratěna J., Fořt I., 2004. Study of the discharge stream from a standard Rushton turbine impeller. *Acta Polytechnica*, 44, 39-47.

Obeid A., Fořt I., Bertrand J., 1983. Hydrodynamic characteristics of flow in systems with turbine impeller. *Coll. Czech. Chem. Commun.*, 48, 568-577.

Ranade V., Perrard M., Sauze N. L., Xuereb C., Bertrand J., 2001. Trailing vortices of Rushton turbine: PIV measurements and CFD simulations with snapshot approach. *Chem. Eng. Res. Des.*, 79, 3–12. DOI: 10.1205/026387601528471.

Schafer M., Hofken M., Durst F., 1997. Detailed LDV measurement for visualisation of the flow field within a stirred-tank reactor equipped with a Rushton turbine. *Chem. Eng. Res. Des.*, 75, 729-736. DOI: 10.1205/026387697524399.

Talaga J., Fořt I., 2012. The velocity field in the discharge stream from a Rushton turbine impeller. *14th European Conference on Mixing*, Warszawa, 10-13 September 2012.

Venneker B.C., Derksen J.J., den Akker H.E.V., 2010. Turbulent flow of shear-thinning liquids in stirred tanks - The effects of Reynolds number and flow index. *Chem. Eng. Res. Des.*, 88, 827–843. DOI: 10.1016/j.cherd.2010.01.002.

Wu H., Patterson G., 1989. Laser-Doppler measurements of turbulent-flow parameters in a stirred mixer. *Chem. Eng. Sci.*, 44, 2207–2221. DOI: 10.1016/0009-2509(89)85155-3.

*Received 23 June 2013*
*Received in revised form 10 February 2014*
*Accepted 17 February 2014*